

Assessing saturation physics explanations of collectivity in small collision systems with the IP-JAZMA model

J.L. Nagle*

University of Colorado Boulder and CEA/PhT/Saclay

W.A. Zajc†

Columbia University

(Dated: August 6, 2018)

Experimental measurements in relativistic collisions of small systems from $p+p$ to $p/d/{}^3\text{He}+A$ at the Relativistic Heavy Ion Collider (RHIC) and the Large Hadron Collider (LHC) reveal particle emission patterns that are strikingly similar to those observed in $A+A$ collisions of large nuclei. One explanation of these patterns is the formation of small droplets of quark-gluon plasma (QGP) followed by hydrodynamic evolution. A geometry engineering program was proposed [1] to further investigate these emission patterns, and the experimental data from that program in $p+\text{Au}$, $d+\text{Au}$, ${}^3\text{He}+\text{Au}$ collisions for elliptic and triangular anisotropy coefficients v_2 and v_3 follow the pattern predicted by hydrodynamic calculations [2]. One alternative approach, referred to as initial-state correlations, suggests that for small systems the patterns observed in the final-state hadrons are encoded at the earliest moments of the collision, and therefore require no final-state parton scattering or hydrodynamic evolution [3, 4]. Recently, new calculations using only initial-state correlations, in the dilute-dense approximation of gluon saturation physics, reported striking agreement with the v_2 patterns observed in $p/d/{}^3\text{He}+\text{Au}$ data at RHIC [5]. The reported results are counterintuitive and thus we aim here to reproduce some of the basic features of these calculations. In this first investigation, we provide a description of our model, IP-JAZMA, and investigate its implications for saturation scales, multiplicity distributions and eccentricities, reserving for later work the analysis of momentum spectra and azimuthal anisotropies. We find that our implementation of the saturation physics model reproduces the results of the MSTV calculation of the multiplicity distribution in $d+\text{Au}$ collisions at RHIC. However, our investigations, together with existing data, call into question some of the essential elements reported in Ref. [5].

I. INTRODUCTION

The standard model for the evolution of the medium in heavy ion ($A+A$) collisions at RHIC and the LHC assumes the matter proceeds through a quark-gluon plasma stage described quantitatively via nearly inviscid hydrodynamics [6]. Observations in $p+p$ and $p/d/{}^3\text{He}+A$ collisions of features similar to those found in $A+A$ collisions raise the question of whether one forms quark-gluon plasma in these smaller systems as well, albeit in a smaller volume and evolving for a shorter lifetime – for recent reviews see Refs. [7–9]. A particularly striking theoretical calculation, with the evocative title *One Fluid to Rule Them All* [10] is the simultaneous matching of viscous hydrodynamic calculations with $p+p$, $p+\text{Pb}$, and $\text{Pb}+\text{Pb}$ data from the LHC using a common set of initial conditions and hydrodynamic input parameters. A geometry engineering program was proposed at RHIC specifically to test the hypothesis that the initial geometry was responsible for the momentum anisotropies by generating droplets with different magnitudes of ellipticity and triangularity via $p+\text{Au}$, $d+\text{Au}$, and ${}^3\text{He}+\text{Au}$ collisions [1]. This program led to experimental measurements by the PHENIX experiment at RHIC [2] that

are found to be in good quantitative agreement with the hydrodynamic predictions.

Since these findings have large impact, it is scientifically mandated to scrutinize the hydrodynamic calculations and their sensitivities to various inputs, while at the same time to fully explore alternative explanations. One such alternative explanation was proposed shortly after the first collective-type signatures were observed in high-multiplicity $p+p$ collisions at the LHC [11]. The calculation is done in the context of gluon saturation physics and finds azimuthal correlations between particles that extend over large rapidity ranges [3, 4]. Many additional papers have followed within this saturation physics framework where the correlations are generated in the initial state, just at the point of interaction, and require no final state interactions amongst produced partons or hadrons as modeled via scattering or fluid flow – for a useful review see Ref. [9].

In the case of initial-state models, a key feature is that the particle correlations are generated within distinct color domains that have a transverse size of order $1/Q_s$ where Q_s is the saturation momentum scale. These domains extend longitudinally, thus giving rise to “ridge-like” correlations long-range in rapidity. It is notable that for $Q_s \approx 1$ GeV, the typical domain transverse size is ≈ 0.2 fm. Thus, even in a $p+p$ or $p+A$ collision, with a saturation scale of order 1 GeV, it is possible to have a number of distinct color domains covering the interaction

* jamie.nagle@colorado.edu

† zajc@nevis.columbia.edu

region. If the various color domains have comparable field strengths, as the number of domains N increases, the correlations decrease. The reason is simply that the domains are uncorrelated in their orientation (in both coordinate space and color space) of the color fields and thus any strong angular correlation from one domain is diluted by particles emitted from other domains with random orientations with respect to the first domain.

In this paper, we focus in particular on the comparison of p +Au and d +Au collisions at RHIC because there is a clear separation of scales. The average separation between the nucleons in the deuteron is $\langle r \rangle = 3.33$ fm which is an order-of-magnitude larger than the typical domain size. In the scenario where individual domains are separately resolved, there is a simple prediction that the correlation or v_2 magnitude should follow

$$v_2(p + Au) > v_2(d + Au) \quad (1)$$

since the incoherent addition of domains from the proton and the neutron in the deuteron simply increases the number of uncorrelated color fields, thereby decreasing their cumulative effect. There appears to be consensus in the field that in the case where the individual domains of transverse size $1/Q_s$ are resolved, the above equation holds. The experimental data definitively rule out this scenario [2].

After the submission of the full experimental data set of $v_2(p_T)$ and $v_3(p_T)$ in high-multiplicity (the highest 5%) p +Au, d +Au, ^3He +Au collisions from the PHENIX collaboration [2], a new manuscript [5] was submitted by Mace, Skokov, Tribedy and Venugopalan (hereafter referred to as MSTV), with postdictions that appear to reconcile initial-state correlations with the experimental data, showing reasonable agreement with the system dependence of $v_2(p_T)$ (though not $v_3(p_T)$). Again, here we focus on the $v_2(p_T)$ differences between p +Au and d +Au for simplicity and attempt to summarize these surprising results, and then test them. Since we are specializing to these asymmetric collisions, in what follows “target” will always refer to the heavier (Au) nucleus, and “projectile” will refer to the proton or deuteron. In cases where it does not cause confusion, we will refer to saturation scales in the proton that will also apply to the neutron in the deuteron.

II. MSTV FRAMEWORK

There are a number of calculational steps and arguments in the MSTV paper [5]; here we provide only a brief summary. The calculation is done in the dilute-dense framework, in contrast to previous IP-Glasma [12] calculations done in the dense-dense framework. Thus the proton or deuteron projectile is considered “dilute” and the target nucleus “dense” in terms of gluon occupation number. In their calculation, MSTV consider a gluon from the target nucleus scattering from color domains in the projectile proton or deuteron. This implies that

the nucleon is in or near a saturated gluon state where one can utilize the weakly-coupled gluon field framework for the nucleon in a region of parton momentum fraction $x \sim 0.01$ relevant for midrapidity hadrons produced with transverse momentum $p_T = 1-3$ GeV/c at RHIC. This is in sharp contrast with the estimate in the original IP=Sat paper by Kowalski and Teaney [13], also at $x = 0.01$, for the proton saturation scale at the center of the proton being $Q_s^2 = 0.67$ GeV². Note that this is the gluon saturation value determined from Kowalski and Teaney’s Figure 25 and the relation they provide between gluon and quark saturation scales. (In the text they quote a value of 1.3 GeV² that appears incorrectly labeled and to be for some smaller x value.) We highlight that $Q_s^2 = 0.67$ GeV² is at the center of the proton, and that integrating over a radius of 0.65 fm the average value is $\overline{Q_s^2} = 0.28$ GeV². These numerical values are of interest because they are sufficiently low to call into question the assumption of the weak coupling limit for the projectile.

MSTV then state that the target gluon will interact with individually resolved color domains (in the proton) if the k_T of the target gluon satisfies $k_T > Q_s(\text{proj})$, i.e., if the gluon from the target is capable of resolving domains in the projectile proton of typical (transverse) size $1/Q_s(\text{proj})$. In the first draft of the MSTV paper this condition is written in terms of p_T , which is also used therein for the magnitude of the transverse momentum of the final-state gluon satisfying $\mathbf{p}_T = \mathbf{k}_T(\text{proj}) + \mathbf{k}_T(\text{targ})$. We have benefited from private communications with the authors that have clarified that the k_T indicated here is for the target gluon alone.

If the target gluon was in fact resolving individual domains in the projectile, one would have the ordering specified in Eqn. 1, which is ruled out by experimental data. However, MSTV argue that if $k_T < Q_s(\text{proj})$ then the target gluon cannot resolve the individual domains in the projectile but instead interacts with a number of order $\sim Q_s(\text{proj})^2/k_T^2$ of domains “simultaneously”, also referred to by MSTV as “coherently.” While this may be the case it appears to be in contradiction with the requirement for the dilute-dense formalism [14] that $Q_s(\text{proj}) < k_T < Q_s(\text{targ})$. In Appendix I, we address the relative magnitude of $Q_s(\text{proj})$ and $Q_s(\text{targ})$ and find no clear separation of scales. This is the first of several areas of tension where we seek greater clarity in the formulation of the MSTV mechanism.

A second such concern involves the MSTV results for v_2 in $p/d/{}^3\text{He}$ +Au, which have an ordering $v_2(d+\text{Au}) > v_2(p+\text{Au})$ up to hadron $p_T \approx 3$ GeV and only there is there a slight hint of the ordering reverting to the pattern of the inequality in Eqn. 1. Does that imply that the typical k_T of a gluon from the projectile, and hence $Q_s(\text{proj})$, is of order $(3 \text{ GeV})/2 = 1.5 \text{ GeV} \Rightarrow Q_s(\text{proj})^2 = 2.25 \text{ GeV}^2$ in the proton at RHIC for $x \sim 0.01$? As discussed below, the MSTV calculation does incorporate fluctuations in the saturation scale, but $Q_s(\text{proj})^2 \sim 2.25 \text{ GeV}^2$ is an order of magnitude larger

than the $\overline{Q_s^2} = 0.28 \text{ GeV}^2$ quoted above. A complete understanding of the calculations presented by MSTV will require clear discussion of the numerical values of all relevant scales. As we will see in the following discussion, it is equally important to understand the physics assumptions behind the implied coherent interactions with color fields over the large distance scales set by the size of the deuteron.

Another key item for investigation is the assertion that with saturation scale fluctuations, and in the dilute-dense framework, the multiplicity N_{ch} of an event, irrespective of whether it is a p +Au or d +Au collision, will be proportional to $Q_s^2(\text{proj})$. Thus, a 5% highest multiplicity d +Au event that has a midrapidity $dN_{ch}/d\eta \approx 18$ will have a higher saturation scale than a 5% highest multiplicity p +Au event that has a $dN_{ch}/d\eta \approx 12$. This is the last critical step that enables not only the ordering of v_n from Eqn. 1 to be negated, but in fact reversed such that $v_2(d\text{+Au}) > v_2(p\text{+Au})$. In the remainder of the paper, we test this assertion and others utilizing the IP-JAZMA framework.

III. IP-JAZMA IMPLEMENTATION

We note at the outset that the goal of the open source IP-JAZMA code is not to re-implement and fully reproduce IP-Glasma or MSTV calculations. In particular, in those complex numerical implementations there are too many algorithmic details and key parameters to be able to reproduce them in exactitude. That project is a critical scientific step that awaits the public release of those codes. For these studies, the goal is to incorporate the identical initial physics steps, to gain insight on the various sources of fluctuations, and to test key statements in MSTV relating underlying variables. To that end, we describe in simple language the step-by-step process in the IP-JAZMA calculation.

A. Monte Carlo Glauber

The first step in the IP-JAZMA calculation, as well as in the IP-Glasma and MSTV implementations, is to run standard Monte Carlo Glauber [15] and for each collision event to output the x,y coordinates (in the plane transverse to the beam axis) of all nucleons. In our calculation, we utilize the publicly available PHOBOS Monte Carlo Glauber code [16]. We use the standard Woods-Saxon parameter sets in the code for the Au nucleus including the hard core repulsive parameter ($d = 0.4 \text{ fm}$), such that nucleons do not completely overlap in three-dimensional space within the nucleus. For the deuteron the Hulthén wavefunction is employed. A key insight from low-energy nuclear physics is that the deuteron is a very loosely bound state of the proton and neutron and the average three-dimensional spatial separation between them $\langle r \rangle = 3.33 \text{ fm}$. In d +Au collisions, the relevant length

scale is the proton-neutron separation in the transverse plane r_T since that defines whether both nucleons undergo inelastic collisions with the target nucleus and how far apart they strike. Figure 1 shows the distribution of r_T from the Hulthén wavefunction; the average value $\langle r_T \rangle = 2.61 \text{ fm}$. The high multiplicity (0-5% centrality) data used in the PHENIX analysis select a subset of d +Au events in which both the proton and the neutron are more likely to strike near the center of the Au nucleus. The precise bias is model-dependent (for example, on the mixture of binary versus participant scaling used to model particle production), but even in the extreme case of N_{coll} scaling $\langle r_T \rangle = 1.66 \text{ fm}$, i.e., there remains a substantial average separation between the neutron and proton. We will further quantify these statements in the context of the IP-JAZMA model in the discussion to follow.

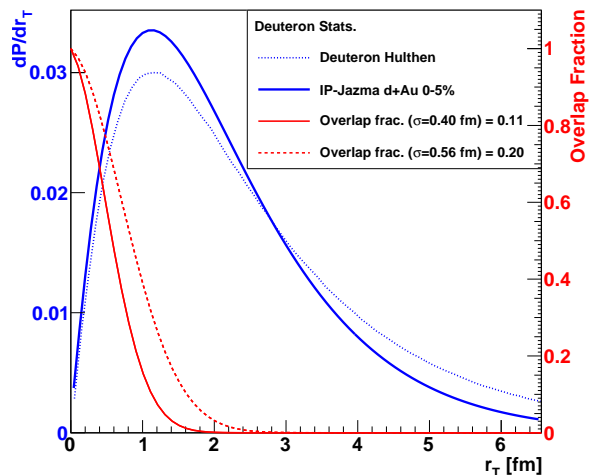


FIG. 1. Two-dimensional separation distance r_T distribution between the proton and neutron constituents of the deuteron. Shown are results from the deuteron Hulthén wavefunction as well as for events selected within the 5% highest multiplicity from the IP-JAZMA dilute-dense calculation. In addition, we calculate the overlap fraction defined in Section III D as a function of r_T between the two nucleons following two-dimensional Gaussian distributions of width $\sigma = 0.40$ and 0.56 fm , and quote the values integrating over the IP-JAZMA distribution.

B. Impact Parameter Saturation (IP-Sat)

Next we follow the Impact Parameter Saturation (IP-Sat) model [13] for setting the gluon saturation scale. In this formulation, the gluon thickness function of the nucleon $T_G(b)$ is a function of the impact parameter, i.e. the radial distance from the center at which one probes the nucleon, and this is assumed to have a simple Gaussian

form

$$T_G(b) = \frac{1}{2\pi B_G} e^{-b^2/(2B_G)} \quad (2)$$

where B_G is determined via fits to electron-proton scattering data at HERA. We highlight that there are different values of B_G in the literature and hence this parameter choice may be significant. One can then solve an implicit equation for the saturation scale squared Q_s^2 as a function of transverse distance from the center of the nucleon in terms of the strong coupling constant $\alpha_s(Q^2)$ and the gluon structure function $g(x, Q^2)$ [17]:

$$Q_s^2(x, b) = \frac{\pi}{3R^2} \alpha_s(Q_0^2 + 2Q_s^2) xg(x, Q_0^2 + 2Q_s^2) e^{-\frac{b^2}{2B_G}} \quad (3)$$

The seemingly odd factors of $Q_0^2 + 2Q_s^2$ that appear here are due to the precise definition of the saturation momentum in terms of the color-dipole radius and the relation between that radius, the initial scale Q_0 and the color-dipole cross section found in the original IP-Sat paper [13]; see also Appendix I in Ref. [18]. The value of $R \equiv \sqrt{B_G} = 0.35$ fm is commonly used [8, 18] which corresponds to the value $B_G = 3.18 \pm 0.4$ GeV⁻² found in Ref. [19], where it is carefully explained that the implied small proton radius is the appropriate value for two-gluon exchange processes [20] [21]. As detailed in Ref. [8], solving Eq. 3 at the x -scale relevant for RHIC energies, one retains to a very good approximation the Gaussian functional form – see Figure 4.5 from that reference – and with a slightly reduced width of $\sigma = 0.32$ fm relevant for collisions at 200 GeV. In practice, this translates into a Gaussian distribution for the squared saturation scale Q_s^2 with a width σ relative to the nucleon center in the transverse plane:

$$Q_s^2(x, y) = Q_{s,0}^2 \times \exp[-r_T^2/2\sigma^2] \quad (4)$$

where $r_T = \sqrt{(x - x_i)^2 + (y - y_i)^2}$ such that x_i, y_i are the center of the i th nucleon in the transverse plane and $Q_{s,0}^2$ is the squared saturation scale at the center of the nucleon.

The imperfect constraints from HERA data, together with the need to use values appropriate for the x -scale of interest, results in some ambiguity in the precise value to select for B_G , which then propagates into the resulting σ for the saturation distribution (Eqn. 4). MSTV (private communication) use the value of $B_G = 4.25$ GeV⁻² found in the original IP-Sat paper [13], resulting in $\sigma = 0.4$ fm. It is clear that in this parameter alone there is a systematic uncertainty of order 10-15%. There is also an unquantified systematic uncertainty in assuming the Gaussian profile of Eqn. 2 is valid at large distances from the center of the proton, rather than an exponential form. The study of possible exponential shapes in Ref. [13] found the effect to be small when considering deep-inelastic scattering on the proton, but this analysis should be revisited in the current context of overlapping color domains between the proton and neutron in the

diffuse deuteron configurations that still dominate the most central 0-5% events in d +Au collisions at RHIC. For the purposes of consistency with MSTV, we will utilize Eqn. 4 with $\sigma = 0.40$ fm throughout the remainder of this work.

We note here that the saturation scale is exactly that, a scale rather than a precise physical quantity. The convention used in Ref. [13] to define it (and adapted by essentially all subsequent papers performing quantitative calculations) is actually framed in coordinate space: the saturation radius r_s and the resulting saturation cross section is the one for which the proton represents one absorption length. The saturation momentum Q_s is then defined via $Q_s^2 = 2/r_s^2$, where the factor of 2 is introduced to maintain consistency with a previous definition of a coordinate-space saturation scale by Golec-Biernat and Wüsthoff [22]. While there are no issues in any formulation which treats the definition of Q_s consistently, it is also clear that plausible alternative definitions of Q_s could differ by as much as factors of $\sqrt{2}$, so comparisons of Q_s to physical momenta of real particles with similar momentum should be viewed as qualitative rather than quantitative in nature. Note that for the purposes of our IP-JAZMA calculations, this overall scale $Q_{s,0}^2$ is simply a normalization that will not be relevant for the overall proportionality calculation of energy density distributions.

C. $Q_{s,0}^2$ Fluctuations

A critical component in the MSTV calculation is the inclusion of $Q_{s,0}^2$ fluctuations on a nucleon-by-nucleon basis. The theoretical basis for such fluctuations was established in Ref. [23]. They were then calculated analytically in Ref. [24] and implemented in Ref. [25] in order to reproduce the N_{ch} distribution in p + p collisions at the LHC in a saturation physics framework. Those authors argue that there may be several non-perturbative effects that contribute to fluctuations in multiplicity, at least one of which, the event-by-event fluctuations in the saturation scale considered here, is non-perturbative and lies outside the conventional framework of the Color Glass Condensate (CGC). They go on to note fluctuations in the saturation scale are critical to the original explanation of the long-range ridge in p + p collisions within the color domain picture [3, 4]. In order to capture these effects, the fluctuations are assumed to follow a log-normal distribution in the variable $\mathcal{Z} \equiv Q_s/\langle Q_s \rangle$

$$P(\mathcal{Z}) d\mathcal{Z} = \frac{1}{\sqrt{2\pi w^2}} \exp\left(-\frac{\log^2(\mathcal{Z}^2)}{2w^2}\right) \frac{2d\mathcal{Z}}{\mathcal{Z}} \quad (5)$$

with w set to a value of 0.5 as used in Ref. [25]. The authors of Ref. [25] define their log-normal distribution in their Eqn. 5 in terms of $Q_s^2/\langle Q_s^2 \rangle$, but their Figure 1 is plotted as a function of $Q_s/\langle Q_s \rangle$. For the chosen value of $w = 0.5$, we have $\langle Q_s \rangle = e^{w^2/8} \sqrt{\langle Q_s^2 \rangle} = 1.03 \sqrt{\langle Q_s^2 \rangle}$, which is a negligible effect. The resulting distribution is

shown as a function of $Q_s/\langle Q_s \rangle$ in Figure 2, and the high-side tail from the log dependence is notable. In fact, the description of the high-multiplicity distribution in $p+p$ collisions relies on the essentially order one fluctuation width of the distribution and the high-side tail where events with $Q_{s,0}^2$ up to 5–6 times the average value (probabilities $6.4\text{--}1.7 \times 10^{-4}$) are selected.

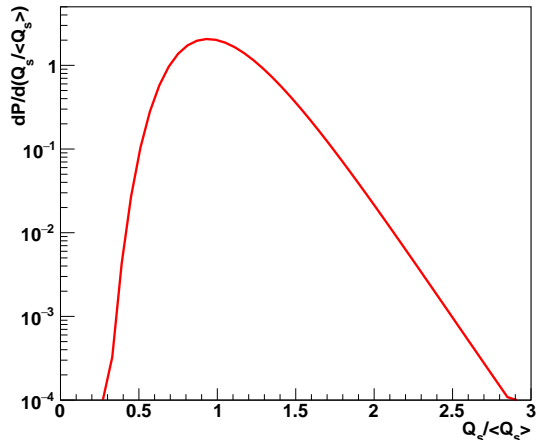


FIG. 2. Functional form for fluctuations in $Q_s/\langle Q_s \rangle$ with standard deviation of 0.5 on $\log[(Q_s/\langle Q_s \rangle)^2]$.

Although not all IP-Glasma calculations invoke such fluctuations, they are critical in the MSTV results. MSTV state that they fit the width of these fluctuations to minimize differences with the STAR $d+Au$ multiplicity distribution at midrapidity [26] and obtain $w = 0.5$, the identical value used to match $p+p$ data at 13 TeV (where the calculation is carried out in the dense-dense limit of IP-Glasma – see more details on this later). It is true that the authors of Ref. [25] comment on the (expected) slow variation of w with energy, but it is striking that precisely the same value in two different formalisms is applicable at RHIC and at LHC energies.

One can quite easily computationally incorporate (or not) such fluctuations for each nucleon in the $Q_{s,0}^2$ value, thus scaling up or down the entire resulting Gaussian distribution from the IP-Sat framework. Note that in doing so the width of the IP-Sat Gaussian in the transverse plane is not changed, only the overall amplitude. The method of incorporating fluctuations in IP-JAZMA is similar to that Ref. [25], where the value of the saturation scale is fluctuated according to Eqn. 5. However, in IP-JAZMA we do not perform any further sampling of local Q_s and/or color charge densities on lattice points in the transverse plane as done in the IP-Glasma model [12]. There is significant debate whether these fluctuations are physically well-motivated, and the improved agreement with multiplicity distributions should not be taken as evidence of such. For example, there are many sources of fluctuations in multiplicity which are not accounted for in the Color Glass Condensate framework - consider multi-

gluon jet processes - and to unambiguously attribute any missing physics to fluctuations in Q_s^2 that are of order 100% with a high side tail would require additional confirmation. It is also striking that the scale of such fluctuations identical in $d+Au$ at RHIC with $x \approx 0.01$ and in $p+p$ at the LHC with particle production dominated by much lower x .

In IP-JAZMA, to find the saturation scale in a collision one simply sums the $Q_s^2(x, y)$ contributions from all nucleons in the projectile to generate a two-dimensional map. The same is done for all nucleons in the target. For illustration, a single $d+Au$ event at 200 GeV event is shown in Figure 3. The left panel shows the two nucleons from the deuteron, each with a perfect Gaussian distribution via IP-Sat. Note that the overall color scale (magnitude) is different for the two nucleons as they represent different random selections from the $Q_{s,0}^2$ fluctuations. The middle panel shows the summed contribution from all the nucleons in the target Au nucleus. At this point the IP-JAZMA calculation should be numerically identical to MSTV for the assumed distribution of Q_s values in the transverse plane.

D. Quantifying Neutron-Proton Overlap

The v_2 ordering of Eqn. 1 relies on the domains in a $d+Au$ being resolved. This is clearly the case when the neutron and proton from the deuteron strike the Au nucleus with a separation between their centers exceeding the color confinement scale. Given the essentially random orientation of the deuteron in the collision, it is of interest to quantify the extent to which the color fields of the neutron and proton overlap in the ensemble of collisions that comprise the 0-5% centrality bin in $d+Au$ collisions. The general form of an expression for the average overlap fraction \bar{f}_s for a distribution $\mathcal{P}(\vec{s})$ of separation in the transverse plane \vec{s} between the proton and neutron centers is

$$\bar{f}_s \equiv \frac{\int f_n(\vec{r} + \frac{\vec{s}}{2}) f_p(\vec{r} - \frac{\vec{s}}{2}) d\vec{r} \mathcal{P}(\vec{s}) d\vec{s}}{\int f_n(\vec{r}) f_p(\vec{r}) d\vec{r}} \quad , \quad (6)$$

where $f_{n,(p)}(\vec{r})$ is a measure of some distribution in the neutron (proton) as a function of distance \vec{r} from its center. This is a reasonable measure of the overlap between the two nucleons; it is 1 when $\mathcal{P}(\vec{s}) = \delta(\vec{s})$, and will decrease with the separation \vec{s} if $f_{n,(p)}(\vec{r})$ is monotonically decreasing with $|\vec{r}|$.

To evaluate the average overlap, we use the essentially Gaussian distribution of the saturation scale in the transverse plane

$$f_n(\vec{r}) = f_p(\vec{r}) = \frac{Q_{s,0}^2}{2\pi\sigma^2} e^{-r^2/2\sigma^2} \quad (7)$$

Doing this, we find that Eq. 6 reduces to

$$\bar{f}_s = \int e^{-s^2/4\sigma^2} \mathcal{P}(\vec{s}) d\vec{s} \quad . \quad (8)$$

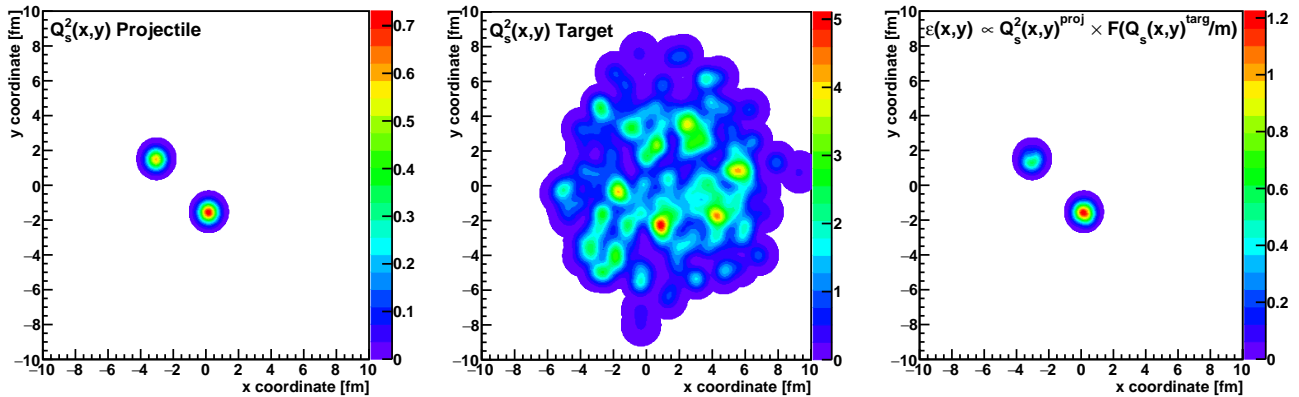


FIG. 3. IP-JAZMA single $d+Au$ interaction event display. Left and middle panels show the $Q_s^2(x,y)$ distribution for the projectile and target nuclei respectively. The right panel shows the calculated energy density from the resulting collision in arbitrary units.

Again, this seems reasonable, e.g., if the two nucleon centers are separated by 2σ , we have $\bar{f}_s = 1/e$. We have computed the numerical value of \bar{f}_s as a function of $|\vec{s}|$ for the distribution of neutron-proton separations for 0-5% $d+Au$ collisions plotted in Figure 1 and plotted the result on the same figure (red curves). For our default value $\sigma = 0.4$ fm, we find only an 11% overlap between the neutron and proton. While extending the saturation distribution with $\sigma = 0.56$ fm changes this value to 20%, it is clear that the distribution of separations between the neutron and proton even in the 0-5% most central $d+Au$ collisions is still dominated by configurations where the neutron and proton are separated by a distance exceeding the color confinement scale and therefore separately resolvable.

E. Energy Density in Dense-Dense Case

In the full IP-Glasma calculation [12], the contribution of each nucleon to the color charge squared per transverse area $g^2\mu^2(x, \mathbf{b}_\perp)$ is assumed to be proportional to the saturation scale $Q^2(x, \mathbf{b}_\perp)$, where \mathbf{b}_\perp is the transverse projection of the impact parameter relative to each nucleon's center. The net color charge squared per transverse area at each lattice point in the transverse plane found by summing over the contributions of all nucleons in the projectile, and separately in the target, is used to define the rms of a Gaussian distribution for the fluctuations in local color charge. After such sampling, the resulting charge distributions are used to calculate the electric and magnetic color fields by solving the Classical Yang-Mills (CYM) equations. The local value of the energy density is then computed from the gluonic fields. It is the lattice site fluctuations in local color charge density which give the IP-Glasma event displays of energy-density their fine-scale spiky visual features. As noted in Ref. [8], the initial spatial scale for the color fluctuations is that of

the lattice spacing and therefore not entirely physical.

The authors of Ref. [8] follow the full IP-Glasma formalism and find that, after averaging over these color fluctuations, one obtains a remarkably simple answer. The resulting energy density at proper time $\tau = 0$ for each lattice site is given by:

$$\varepsilon(x, y) \propto g^2 Q_s^2(x, y)_{proj} \times Q_s^2(x, y)_{targ} \quad (9)$$

where g is the strong coupling. (Important discussions on the time evolution away from $\tau = 0$ and the dependence on the lattice spacing may be found in Ref. [27].) We note that in some of the saturation physics literature, factors of g are absorbed into the definition of the saturation scale.

This result is essentially number of collisions N_{coll} scaling for the energy density, i.e. it is the product of the projectile and target thickness functions – only the modest non-linearities in Eqn. 3 prevent this from being strictly true. Note that N_{coll} scaling in traditional Monte Carlo Glauber calculations treat all nucleon-nucleon binary collisions equally; as a result scaling by N_{coll} does not match the expected energy density distribution. However, in this case, the thickness functions include a version of an impact parameter dependence for each nucleon-nucleon interaction, i.e. more peripheral N-N interactions have a smaller overlap of their IP-Sat Gaussian distributions. In that sense, this physics scaling is very similar to Monte Carlo Glauber with constituent quarks that essentially give an impact parameter dependence to nucleon-nucleon interactions [28]. In the publicly available TRENTO model [29], the authors populate arbitrary Gaussian distributions for projectile and target nucleons and find, in the so-called “ $p=0$ geometric” mode, that the resulting energy density is proportional to $\sqrt{T_A \times T_B}$, where $T_{A,B}$ are the nuclear thickness functions. The square-root is arbitrary and as formulated does not represent N_{coll} scaling, but again this approach does incorporate a variant of an impact parameter dependence for N-N interactions.

Thus, for certain parameter selections TRENTO $p = 0$ approximately reproduces the IP-Glasma $A+A$ eccentricities $\varepsilon_2, \varepsilon_3$ – see Figure 3 from Ref. [29].

The result in Eqn. 9 is obtained from the full IP-Glasma gluon field calculation followed by averaging over the fluctuations induced by the Gaussian sampling of color charge on each lattice site. Typical lattice grids used in IP-Glasma calculations are of order 0.025×0.025 fm². One can ask quantitatively when and if these fluctuations are a significant or insignificant contributor to various physics observables – a question that is not asked often enough. For example, Figure 4.7 from Ref. [8] shows for Au+Au collisions at 200 GeV the eccentricities ε_n for $n = 2-6$ obtained after averaging over the lattice-sized color fluctuations match almost perfectly with the full IP-Glasma calculations [18]. This is particularly notable for impact parameter $b = 0$ where fluctuations dominate. We reproduce those results in Figure 4 and compare to IP-JAZMA results in the dense-dense limit using the simple result in Eqn. 9. Overall, there is very good agreement between the IP-Glasma and IP-JAZMA results for the various eccentricities. For more peripheral collisions $b > 8$ fm, there are small deviations for the higher moments $n \geq 4$ which could be related to these additional lattice site fluctuations or parameter choices such as the assumed maximal extent of the IP-Sat Gaussian distribution, as discussed below.

There are a few additional items to mention in this regard. Functionally in the algorithm there is a choice for how far to extend the IP-Sat Gaussian, referred to as r_{max} . Calculations can be sensitive to r_{max} and often extend this to the edge of the entire lattice grid. This choice can influence the eccentricities which could also help explain the differences in more peripheral collisions mentioned above. The IP-Sat assumption of a Gaussian form and parameter setting from HERA data is very unlikely to have any constraint on the tail of the distribution for distances from the center of the nucleon exceeding $(2-3)\sigma \sim (0.8-1.2)$ fm and thus any observable sensitive to choices in r_{max} beyond this must be viewed as systematic uncertainties. In the IP-JAZMA case, we set $r_{max} = 3.0 \times \sigma$ in all results shown here. In the comparison for Au+Au eccentricities as a function of impact parameter mentioned above, there is also the question of what defines the limit of an inelastic collision. If one extends the IP-Sat Gaussian out further, one effectively has a larger inelastic cross section. Various schemes for matching the experimental total $A+A$ inelastic cross section are discussed in Ref. [30]. One last item is that in some papers, the factor g^2 in Eqn. 9 is allowed to run with Q^2 and is evaluated at the maximum value on the lattice site between $Q_s(\text{proj})$ and $Q_s(\text{target})$. This is not standard across IP-Glasma papers, and the g^2 is treated as a constant in the IP-JAZMA calculations shown in this paper.

Before proceeding to a discussion of the dilute-dense limit used in MSTV, we note that there have been several calculations for small systems using the dense-dense

limit in the IP-Glasma framework, including setting initial conditions for $p/d/{}^3\text{He}+A$ collisions [31, 32] and calculating small system multiplicity and momentum distributions [33, 34].

F. Gluon Density in Dilute-Dense Case

The calculation of MSTV is performed in the dilute-dense limit of saturation physics. The authors use the same procedure of Monte Carlo Glauber and IP-Sat [13] deployed in the IP-Glasma framework [12], including the treatment of fluctuations. However, for the subsequent evolution of the gluon field they employ the dilute-dense formalism. appropriate for small systems incident on heavy targets. While the dilute-dense limit was initially developed for $p+\text{Pb}$ collisions Refs. [35, 36], it is applicable whenever one system (the projectile) has a saturation scale significantly lower than that of the other system (the target), i.e. $Q_s(\text{proj}) < Q_s(\text{targ})$. Care must be taken to ensure correct treatment of the odd angular harmonics necessary for the generation of $v_3(p_T)$ [37]. In general, the dilute-dense formalism is considered valid when the $Q_s(\text{proj}) < k_T < Q_s(\text{targ})$. As noted at the end of the previous section, while this may seem quite natural for the treatment of $p+\text{Au}$ and $d+\text{Au}$ collisions at RHIC, reasonable results have also been obtained working in the dense-dense limit for these systems.

In the dilute-dense formalism, after averaging over color fluctuations, the local gluon density is given by

$$N_g(x, y) \propto g^2 Q_s^2(x, y)_{proj} \times F(Q_s(x, y)_{targ}/m) \quad (10)$$

where m is the infrared cutoff applied in the calculation. The function $F(u)$ is taken as

$$F(u) = \int_0^u dy [1 - e^{-y^2}]/y \quad (11)$$

where $u = Q_s(\text{targ})/m$ [38]. As shown in Figure 5, the function $F(u)$ is clearly logarithmic in (Q_s/m) at large values of Q_s/m .

We take the same numerical value $m = 0.3$ GeV as used in MSTV, which was selected in order to best match the $d+\text{Au}$ multiplicity distribution. MSTV cites an earlier IP-Glasma paper relating to systematic uncertainties from this parameter variation, though in that paper they only vary m from 0.1 – 0.2 GeV. We note that in IP-JAZMA we find very little sensitivity to this parameter. Figure 3 (right panel) shows a single $d+\text{Au}$ event and the energy density in arbitrary units calculated using this dilute-dense formulation.

G. Gluons and Energy Density

For calculating initial spatial eccentricities, the above formalism is complete within IP-JAZMA. For matching experimentally measured charged hadron multiplic-

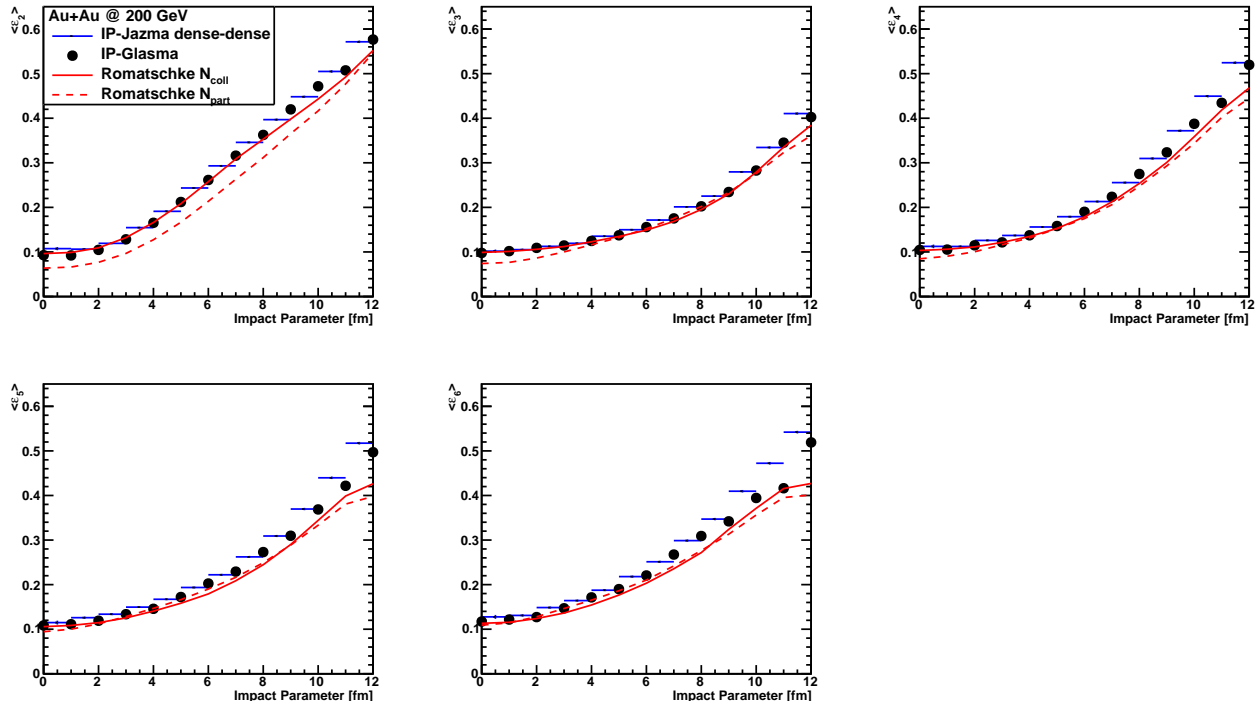


FIG. 4. Calculations of eccentricity moments $\varepsilon_2-\varepsilon_6$ for Au+Au collisions at 200 GeV. Shown are results from the full IP-Glasma calculation [18] compared with calculations from the IP-JAZMA code. Also shown are calculations from Ref. [8] in the N_{coll} and N_{part} cases, noting that the N_{coll} case is the same algorithm as in IP-JAZMA modulo issues such as the r_{max} cutoff.

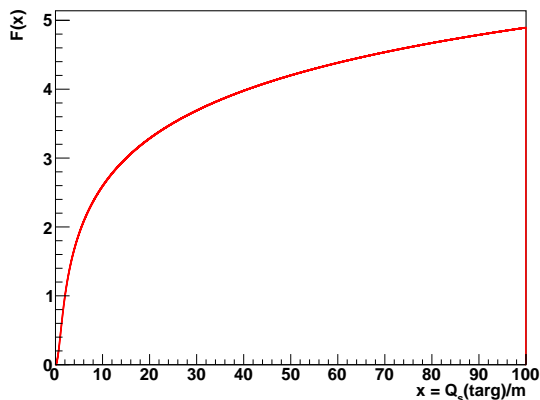


FIG. 5. Functional form $F(x)$ where $x = Q_s(targ)/m$.

ity distributions, IP-JAZMA faces the same issues confronting any theoretical model. The experiments do not measure all neutral hadrons, there are experimental acceptance and efficiency effects including a low- p_T cutoff, and there are mapping issues from gluons to hadrons and associated fluctuations. Renormalizing the distributions relative to the mean quantity, e.g. $N_g/\langle N_g \rangle$ can ameliorate some of these effects, but does not eliminate issues in the shape of the distribution. For example, an ex-

periment measuring hadrons over two units of rapidity will on average measure twice the particles relative to an experiment measuring over one unit (assuming one is on the rapidity plateau). However, rescaling the distribution by a factor of two will not bring the shapes into agreement as there will be a wider distribution in the smaller acceptance case.

That said, for comparing with the MSTV results, within IP-JAZMA, we simply assume that the number of gluons is linearly proportional to the energy density, and therefore will take Eqn. 9 and Eqn. 10 (after summing over lattice sites) as proportional to the number of charged hadrons in the applicable dense-dense and dilute-dense limits respectively. In this initial treatment we defer questions of energy density versus entropy density, given our reasonable description of the $d+Au$ multiplicity distribution (Figure 9), and our goal of understanding the role of various sources of fluctuations in the MSTV calculation. While there are multiple places where fluctuations come into these calculations, it is our intent here to test the contributions of fluctuations just from Monte Carlo Glauber and IP-Sat $Q_{s,0}^2$ fluctuations in order to understand the importance of other sources of fluctuations within MSTV.

IV. IP-JAZMA RESULTS

We begin with the simplest results from IP-JAZMA for light systems and then systematically explore their implications. First consider p +Au collisions at RHIC treating the system in the dilute-dense limit, with no $Q_{s,0}^2$ fluctuations. In all cases the width of the IP-Sat Gaussian $\sigma = 0.40$ fm, the $r_{max} = 3.0 \times \sigma$ within IP-Sat, the infrared regulator $m = 0.3$ GeV and we assume a constant value for g^2 as it appears in Eqn. 10. Note that the exact numerical value of the average $Q_{s,0}^2$ does not enter since we will compute the number of gluon distribution relative to the average number of gluons ($N_g/\langle N_g \rangle$) as done in MSTV. For distributions showing the dependence of $Q_{s,0}^2$ with various parameters we have chosen $Q_{s,0}^2 = 0.67$ GeV² as per previous discussion of this value taken from Ref. [13].

The resulting distribution for $N_g/\langle N_g \rangle$ in p +Au collisions is shown in Figure 6. The distribution has a peak for very low gluon number, in cases where the proton strikes the edge of the nucleus. The distribution then has a somewhat stronger peak near the maximum value, relative to the mean, corresponding to those cases where the proton hits the “thick-enough” part of the target nucleus to “free” all the gluons in the proton. For such configurations, the number of gluons is only logarithmically dependent on the target thickness and one cannot generate any more multiplicity.

Now we perform the identical calculation but with the inclusion of $Q_{s,0}^2$ fluctuations for all nucleons – in both the projectile proton and the target nucleons. The resulting gluon distribution is shown in Figure 7 (left panel). One immediately sees that the shape of the distribution is qualitatively different, being effectively dominated by the choice of magnitude and shape of the $Q_{s,0}^2$ fluctuations. The blue dashed line indicates the selection on the highest 5% multiplicity events.

Since this is a Monte Carlo calculation, we can calculate the average value for $Q_{s,0}^2$ in the proton for all events falling into a particular gluon multiplicity selection. These values are shown in Figure 7 (right panel). Again, the mean value is arbitrary at this point; the key take-away message is that the gluon multiplicity essentially depends linearly on the proton $Q_{s,0}^2$ value. The only deviation is at low multiplicity when the proton hits the edge of the nucleus. This is completely consistent with the statement in MSTV that in the dilute-dense limit there is this simple proportionality $N_{gluon} \propto Q_{s,0}^2$. In selecting the highest 5% multiplicity events, we find in IP-JAZMA that in p +Au collisions at RHIC the average $Q_{s,0}^2$ is higher by a factor of $1.68/0.76 = 2.2$ than the average.

We now move to the d +Au case and show in Figure 8 the distribution of $N_{gluon}/\langle N_{gluon} \rangle$ in the dilute-dense case and without $Q_{s,0}^2$ fluctuations. In this case, the distribution has two peaks away from zero. The peak around $N_g/\langle N_g \rangle \approx 0.8$ corresponds to when only one nucleon from the deuteron hits the target nucleus and in a

thick enough region to fully free the projectile (single nucleon) gluons. Due to the large size of the deuteron, the relative size of this first peak is substantial. The other peak around $N_g/\langle N_g \rangle \approx 1.7$ is produced when both nucleons from the deuteron hit the thick region of the target nucleus.

Next we calculate the gluon distribution for d +Au collisions in the dilute-dense case and with the prescribed $Q_{s,0}^2$ fluctuations, shown in Figure 9. The key observation is that the IP-JAZMA results agree almost perfectly with the MSTV calculation. This IP-JAZMA result in itself is quite remarkable and indicates that by far the dominant source of fluctuations come from Monte Carlo Glauber in combination with $Q_{s,0}^2$ fluctuations which are non-perturbative and lie outside the CGC framework [25]. This is in sharp contradistinction to other sources related to color fluctuations and any “remarkable” derivation of negative binomial fluctuations in the Color Glass Condensate framework [39]. (See also Appendix II in this regard.) Note that in the IP-JAZMA result there are absolutely zero free parameters in the sense that each numerical value, where applicable, exactly matches those used by MSTV.

Also shown in Figure 9 are charged hadron data within $|\eta| < 1.0$ from the STAR collaboration [26]. The MSTV calculation was matched to this distribution with three parameters, the infrared cutoff $m = 0.3$ GeV, the width $w = 0.5$ of the $Q_{s,0}^2$ fluctuations in $\log[(Q_{s,0}^2/\langle Q_{s,0}^2 \rangle)^2]$, and the scale factor relating the saturation scale and the color charge density [5]. Both IP-JAZMA and MSTV reproduce the data reasonably, with the only discrepancy being the significant over-prediction in both for the 0.5% highest multiplicity events. We have verified in IP-JAZMA that this over-prediction is directly related to the width w in Eqn. 5; changing $w = 0.5 \rightarrow 0.45$ provides a good description of the very high multiplicity tail, at the expense of slightly worsened agreement with the data in the region $N_g/\langle N_g \rangle \sim 1-4$.

In the right panel of Figure 9 we show the average $Q_{s,0}^2$ for the neutron and proton from the projectile deuteron as a function of event multiplicity category. As in the p +Au case, there is a linear relationship between N_{gluon} and $Q_{s,0}^2$ once both projectile nucleons move inside the edge of the target nucleus. The 5% highest multiplicity d +Au events have an enhancement in $Q_{s,0}^2$ by $1.31/0.76 = 1.7$, which is lower than the enhancement ratio of 2.2 found in the 5% highest multiplicity p +Au events. This is to be expected from basic probability arguments under the assumption that the neutron and proton in the deuteron fluctuate separately. In these figures, we have followed MSTV in presenting the multiplicity results after scaling $\langle N_{gluon} \rangle$, but of course we know the numerical value for the average value. We find in IP-JAZMA that the 0-5% d +Au events have a multiplicity that is 1.5 times higher than the 0-5% p +Au events. This is very consistent with the ratio of PHENIX experimental measurements of $dN_{ch}/d\eta$ at midrapidity between the 5% most-central d +Au and p +Au events.

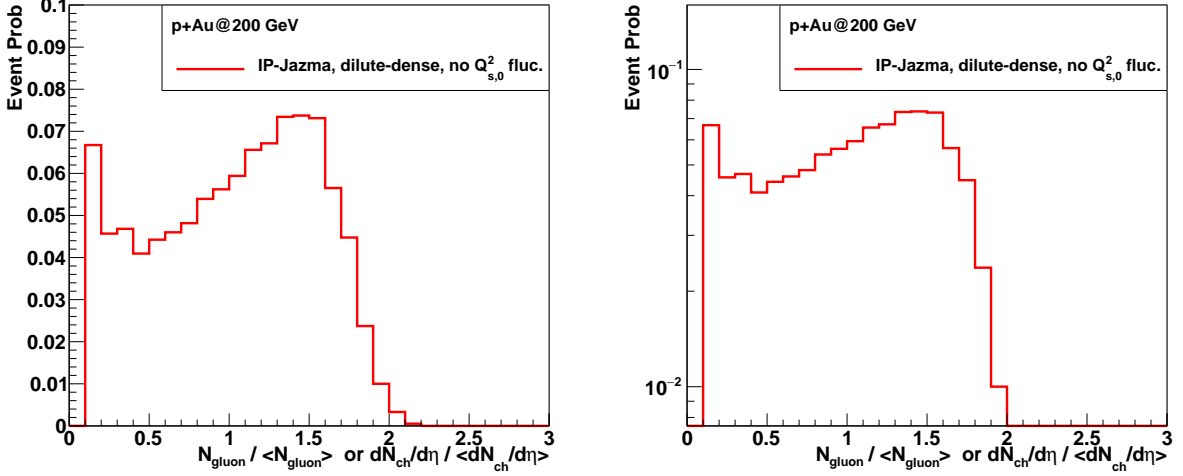


FIG. 6. IP-JAZMA result for the distribution of $N_g / \langle N_g \rangle$ in the dilute-dense case and with no $Q_{s,0}^2$ fluctuations. The left (right) panel has the y-axis on a linear (log) scale.

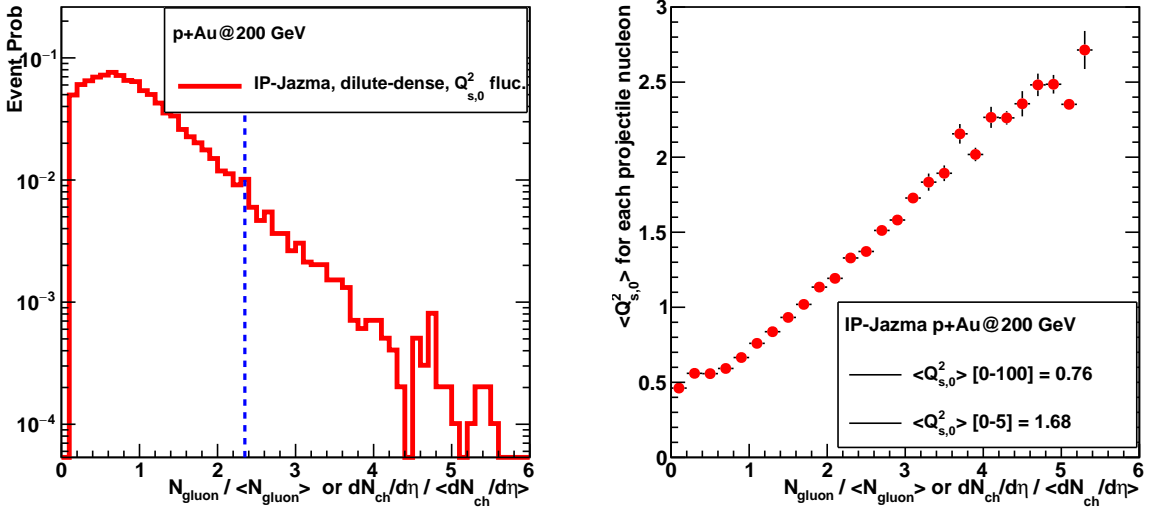


FIG. 7. IP-JAZMA results in $p+Au$ collisions for the distribution of $N_g / \langle N_g \rangle$ in the dilute-dense case and with the inclusion of $Q_{s,0}^2$ fluctuations. The blue dashed line indicates the cutoff for the 5% highest multiplicity events. The right panel shows the average projectile proton $Q_{s,0}^2$ as a function of event selected $N_g / \langle N_g \rangle$.

V. DISCUSSION AND ANALYSIS

In order to further develop our understanding using IP-JAZMA, we define on an event-by-event basis the net interaction area by summing the area of all lattice sites with a deposited energy density above some minimum value ε_{min} . Although ε_{min} is arbitrary, we apply the identical definition to all events in both $p+Au$ and $d+Au$ cases and find that our conclusions are insensitive to this value. Given this well-defined area, one can calculate the average squared saturation scale for the projectile $(Q_s^{proj})^2$ over that area. Figure 10 shows the average

area in both $p+Au$ and $d+Au$ collisions as a function of N_g , where the x-axis is in arbitrary absolute units but the scaling is common for both $p+Au$ and $d+Au$. The yellow circles indicate the region in the middle of the 5% highest multiplicity selection for each collision system.

Quantitatively extracting values for the 5% highest multiplicity events in both collision systems yields average areas of 2.81 and 4.52 fm² in $p+Au$ and $d+Au$ respectively. Similarly, the average values for $(Q_s^{proj})^2$ over those areas are 0.56 and 0.53 GeV² in $p+Au$ and $d+Au$ respectively. Thus, the multiplicity is 1.5 times higher in high multiplicity $d+Au$ compared with

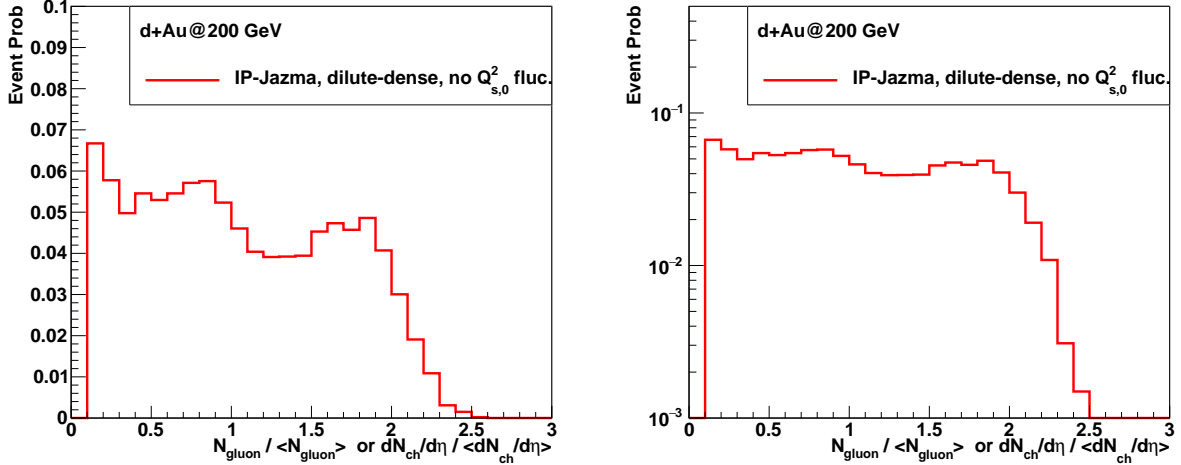


FIG. 8. IP-JAZMA $d+Au$ minimum bias results for the distribution of $N_g/\langle N_g \rangle$ in the dilute-dense case and with no $Q_{s,0}^2$ fluctuations. The left (right) panel has the y-axis on a linear (log) scale.

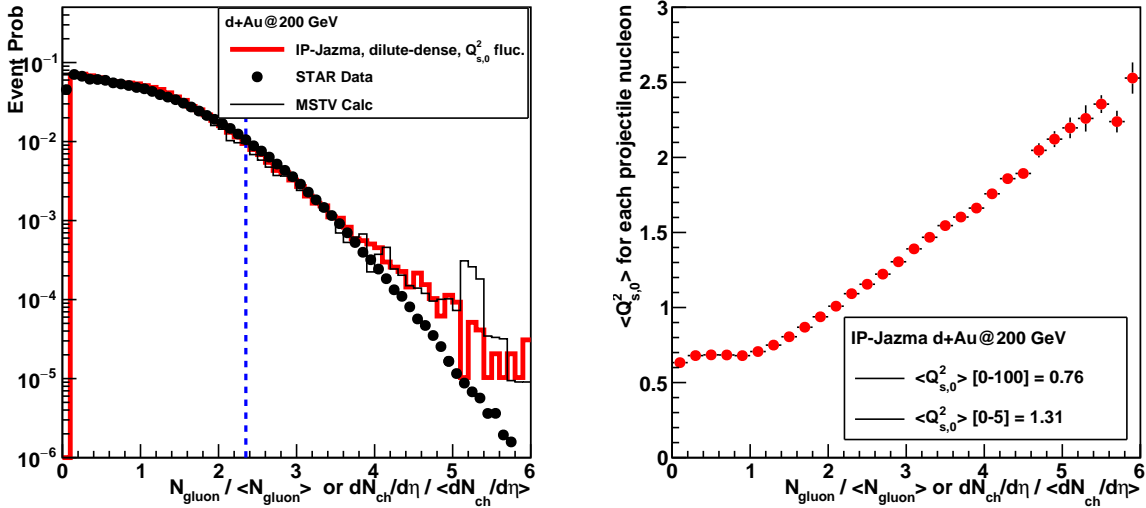


FIG. 9. IP-JAZMA results in $d+Au$ collisions for the distribution of $N_g/\langle N_g \rangle$ in the dilute-dense case and with the inclusion of $Q_{s,0}^2$ fluctuations. The blue dashed line indicates the cutoff for the 5% highest multiplicity events. The right panel shows the average projectile proton $Q_{s,0}^2$ as a function of event selected $N_g/\langle N_g \rangle$.

$p+Au$ (consistent with observations, as noted above) because the area is larger in roughly that same ratio $(4.52 \text{ fm}^2)/(2.81 \text{ fm}^2) \approx 1.6$, while the saturation scale remains the same. This is exactly the opposite of the statement in MSTV, who argue in a similar comparison of $^3\text{He}+Au$ to $p+Au$ collisions that in the dilute-dense limit the higher multiplicity found in 0-5% $^3\text{He}+Au$ collisions results from a corresponding increase in saturation scales $(Q_s^{proj})^2|_{^3\text{He}} > (Q_s^{proj})^2|_p$. In contrast, the IP-JAZMA result makes intuitive sense. If the two nucleons are of order 2 fm apart when striking the target, they represent two essentially independent proton(neutron)+Au collisions and the saturation scale in the two regions is

roughly the same. Thus, the statement in MSTV that in the dilute-dense framework the multiplicity N_{ch} scales with Q_s^2 in the projectile is potentially misleading. It is roughly true for a single system (see RHS of Figure 10), but it is clearly not true *across different systems*. Moreover, the dominant source of higher multiplicity events in $d+Au$ collisions is increases in the geometric overlap rather than increases in the saturation scale of the projectile.

These results and conclusions are consistent with our previous findings. Certainly in the case of an infinite target nucleus being struck by two projectile nucleons that are 1 meter apart it is obvious that the projectile

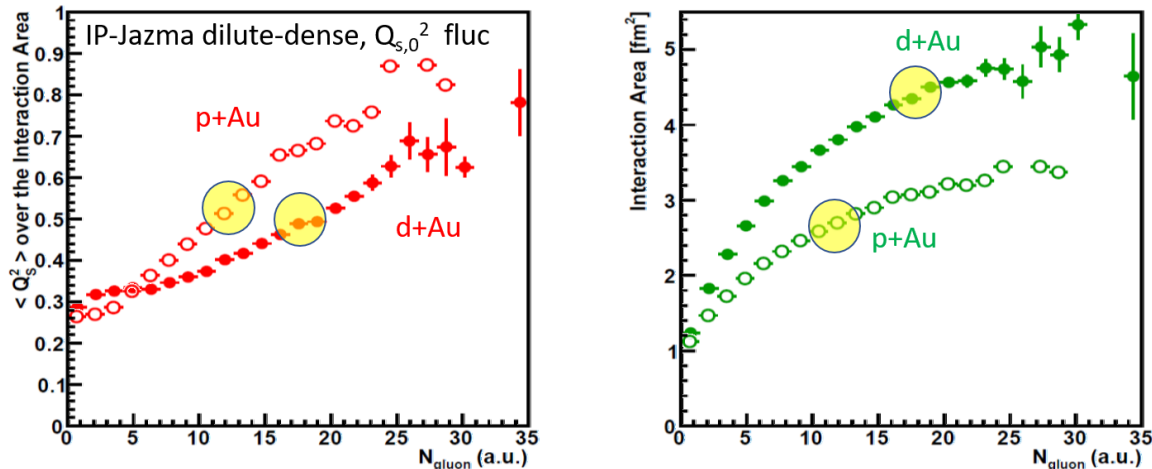


FIG. 10. IP-JAZMA calculations of the interaction area (right) and the average $\langle Q_s^p \rangle^2$ for the projectile over that area (left) as a function of the number of produced gluons N_g in arbitrary absolute units. While arbitrary, the x -axis units are such that one can make a direct comparison between the $p+Au$ and $d+Au$ results. The yellow circles indicate the approximate location for the 5% highest multiplicity selection in both cases, demonstrating that high multiplicity $d+Au$ events result from a larger net interaction area than in $p+Au$ events (RHS), but with similar saturation scales (RHS). See text for further discussion.

saturation scale will be identical to the case when one nucleon hit the target, but the area is simply twice as large. While the Au nucleus is far from infinite, our results presented in Section IIID show that for the loosely bound deuteron, separations of more than 2 fm between the nucleon centers are qualitatively the same as 1 meter, this of course simply being a statement of the confinement scale. In the $d+Au$ collisions, there of course can be configurations where the two nucleons are one behind the other as they impact the target; in such cases the area will be the same and the projectile saturation scale will be larger. However, these configurations are quite suppressed by phase space, and in the full IP-JAZMA calculation for the $d+Au$ 5% highest multiplicity events the average transverse separation is reduced slightly from the unbiased average, but is still greater than 2 fm, consistent with the arguments presented above.

VI. MSTV PREDICTION

Putting aside for the moment the issues elucidated above, there is a prediction explicitly stated in the MSTV paper. Since the assertion is that the anisotropies for $k_T < Q_s^{proj}$ are from interactions that are coherent over multiple domains in the projectile, the anisotropies scale with Q_s^{proj} . As noted in the previous section, the authors also state that in the dilute-dense framework the multiplicity N_{gluon} scales with $(Q_s^{proj})^2$. As a result, MSTV predict that if $p+Au$ and $d+Au$ events are selected with the same $dN_{ch}/d\eta$ then the v_2 and v_3 magnitudes and p_T dependence should be “identical”. However, this statement is contradicted by PHENIX data on

$d+Au$ v_2 values in different multiplicity classes [40] extant at the time of the MSTV submission. The $d+Au$ 20-40% centrality, as defined by the multiplicity in the PHENIX Beam-Beam Counter covering pseudorapidity $-3.9 < \eta < -3.1$ (i.e. in the Au-going direction), has a midrapidity $dN_{ch}/d\eta = 12.2 \pm 0.9$ and is essentially identical to the $p+Au$ 0-5% centrality with a midrapidity $dN_{ch}/d\eta = 12.3 \pm 1.7$ [41]. The comparison of $v_2(p_T)$ values is shown in Figure 11 and highlights that the anisotropies are not the same – thus contradicting the finding of MSTV.

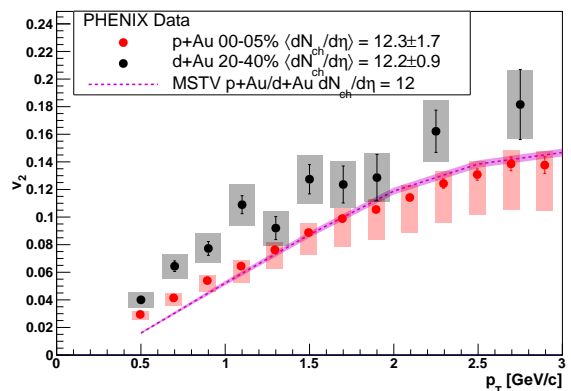


FIG. 11. PHENIX published data for v_2 in $p+Au$ and $d+Au$ collisions in 0-5% and 20-40% multiplicity selections, which have comparable average $dN_{ch}/d\eta$ values as shown. Also shown is the MSTV calculation for $p+Au$ at this multiplicity, which should be identical to their result for $d+Au$ 20-40% multiplicity since the $dN_{ch}/d\eta$ is essentially the same.

VII. OTHER ISSUES

The MSTV calculation produces striking agreement of the $v_2(p_T)$ distributions for the 5% highest centralities in p +Au, d +Au and ^3He +Au collisions, as shown in Figure 4 of their paper. However their calculations are for the p_T of the *gluon*, while the data are of course for charged hadrons. As shown in Figure 7 of an IP-Glasma calculation of the hadron momentum spectrum [33] the gluon p_T distribution is strikingly different from the hadron p_T distribution – an order of magnitude below it at 0.5 GeV/c and an order of magnitude above at 3.0 GeV/c. The inclusion of a hadronization scheme is required to roughly reproduce the experimental data in p + p collisions at the LHC. Its omission in MSTV is notable since other studies with IP-Glasma + PYTHIA include a model dependent version of this hadronization [34]. These observations are not original, and in fact are supported by previous statements of a subset of the MSTV authors: “*Fragmentation of gluons into hadrons will further soften the signal [42]. Our results (for v_n) therefore represent maximal values for azimuthal correlations in this initial state framework . . . Energy evolution of parton distributions and parton to hadron fragmentation will decrease the values (of $v_2(m)(p_\perp)$) shown.*” [43]

Another argument that appears in the MSTV paper concerns the relationship between the k_T of a gluon from the target and its ability to resolve color domains in the projectile. In the scenario of the dilute-dense limit, MSTV state that those gluons from the target nucleus satisfying $k_T < Q_s^{proj}$ will interact coherently with $(Q_s^{proj}/k_T)^2$ domains in the projectile. As noted previously, we find that the Q_s^{proj} values are nearly the same in the 0-5% highest multiplicity events with deuteron and proton projectiles. This observation appears to invalidate the MSTV finding of resulting larger v_2 anisotropies in d +Au compared with p +Au. While the inclusion of fluctuations in $Q_{s,0}^2$ increases the average Q_s^{proj} in the 0-5% highest multiplicity events, as seen in Figure 10, these values never approach numbers comparable to $Q_s^{proj} \approx 1.5\text{--}3$ GeV, or equivalently $(Q_s^{proj})^2 \approx 2.25\text{--}9$ GeV². This is a critical observation because the system ordering shown in Figure 3 of the MSTV paper indicates that individual domains are not resolved in the projectile all the way up to $p_T \approx 2.5\text{--}3.0$ GeV. That is, even in the presence of fluctuations, the arguments of MSTV appear to require saturation scales in the projectile well in excess of those calculated with IP-JAZMA in p +Au and d +Au collisions at RHIC energies.

VIII. SUMMARY

We have constructed the IP-JAZMA model, which provides a very simple implementation of saturation physics phenomenology in the context of Glauber modeling of nuclear collisions. Using this model, we have studied basic

aspects of the dense-dense and dilute-dense frameworks for the CGC in the context of the recent publication by MSTV. We summarize our findings:

1. The restriction to the 0-5% centrality bin introduces only a mild bias on the average transverse separation between the neutron and proton on the face of the Au nucleus in d +Au collisions (Section III A). A quantitative measure of the overlap between the neutron and proton gluon distributions in this centrality class suggests the overlap contribution is at most 20% and more probably 11% (Section III D).
2. IP-JAZMA, following the simple prescription found in Ref. [8], provides an excellent description of the eccentricity moments ϵ_2 through ϵ_6 over most of the full range of impact parameters in Au+Au collisions, reproducing the results for all but the most peripheral collisions of the full IP-Glasma calculation (Section III E).
3. Using the simplest possible implementation of fluctuations in the saturation scale (Section III C), IP-JAZMA produces a description of the multiplicity distribution in d +Au collisions identical to that calculated by MSTV (Section IV).
4. IP-JAZMA provides unequivocal support for the intuitive argument that the dominant source of higher multiplicities in d +Au collisions is through increases of the interaction area from quasi-independent collisions of the neutron and proton from the deuteron, rather than through local increases in the saturation scale (Section V). While MSTV do not address this issue directly, their prediction that equal multiplicity p +Au and d +Au collisions should have identical $v_2(p_T)$ and $v_3(p_T)$ due to the same saturation scale, rests on the underlying assumption that the dominant source of higher multiplicity is via increases in the saturation scale.
5. That same prediction by MSTV is invalidated by existing experimental data for $v_2(p_T)$ in p +Au and d +Au collisions (Section VI)
6. We are unable to reconcile the good agreement MSTV present between $v_2(p_T)$ for *gluons* and the PHENIX data for hadrons with the decorrelations both in momentum and angle expected from gluon to hadron fragmentation. In addition, the MSTV argument appears to require saturation scales in p +Au and d +Au collisions well in excess of those we calculate for these collisions at RHIC energies (Section VII).

More generally, our IP-JAZMA calculations suggest that many features attributed to *local* color fluctuations and *ab initio* features of the CGC are not needed to reproduce multiplicities and eccentricities in nuclear collisions at RHIC. In future work we intend to extend IP-JAZMA to include calculation of momentum spectra and

azimuthal anisotropies. It may well be that this extension fails, indicating that features intrinsic to the CGC approach are needed for these more microscopic observables. Until then, it will not be possible to test the nature of the coherent correlations over domains and their numerical implementation, including the exact parameter values, with the information available in MSTV. The proven way to perform scientific assessments of technically involved calculations is through open-source code, as demonstrated by continuing advances in hydrodynamics and jet energy loss. It is our hope that this first IP-JAZMA work will be useful in that effort.

ACKNOWLEDGMENTS

We are pleased to acknowledge very useful discussions with Jean-Paul Blaizot, Francois Gelis, Giuliano Giacalone, Constantin Loizides, Cyrille Marquet, Darren McGlinchey, Al Mueller, Bjoern Schenke, and Hugo Pereira da Costa. We thank Tuomas Lappi, Jean-Yves Ollitrault, and Paul Romatschke for a careful reading of the manuscript. We also would like to thank the MSTV [5] authors Mark Mace, Vladimir Skokov, Prithwish Tribedy, and Raju Venugopalan for their detailed descriptions of their calculation and their patient answers to our various questions. JLN and WAZ gratefully acknowledge funding from the Division of Nuclear Physics of the US Department of Energy under grants DE-FG02-00ER41152 and DE-FG02-86ER40281, respectively. JLN is also thankful for generous support from CEA/IPhT/Saclay during his sabbatical time in France.

IX. APPENDIX I

Here we briefly revisit the question of applying the dense-dense or dilute-dense frameworks. As mentioned previously, the dilute-dense framework should be applicable when $Q_s(\text{proj}) < k_T < Q_s(\text{targ})$, which may seem natural in the case of $p+\text{Au}$ or $d+\text{Au}$ collisions. However, a number of IP-Glasma results in the dense-dense limit have been published by some of the same authors and applied also to $p+\text{Au}$ and $d+\text{Au}$ collisions at RHIC, as well as to $p+p$ and $p+\text{Pb}$ collisions at the LHC. Given that in MSTV, while working in the dilute-dense limit, significant fluctuations are added to the saturation scale, it is interesting to check the validity of the condition for applicability of this limit. For the 5% highest multiplicity $d+\text{Au}$ events, we compare the ratio of $Q_s^2(\text{proj}) / Q_s^2(\text{targ})$ weighted by the gluon density given in Eqn. 10. The results are shown in Figure 12. The distribution has a peak at ≈ 0.4 (corresponding to $Q_s(\text{proj}) \sim 0.6 Q_s(\text{targ})$), but is quite broad, with the mean of the distribution at ≈ 0.8 , approaching and sometimes exceeding the regime where the saturation scales are equal. Although the condition for the dilute-dense limit is expressed as a simple inequality, ideally the scales

should be well-separated rather than comparable.

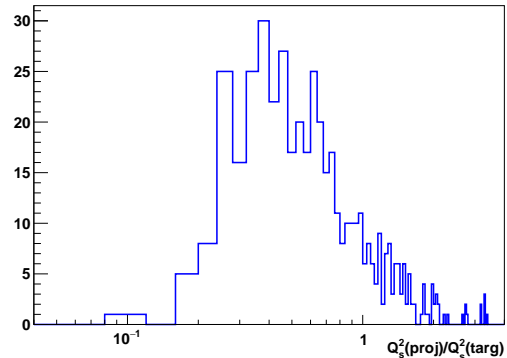


FIG. 12. IP-JAZMA $d+\text{Au}$ highest multiplicity 5% distribution for $Q_s^2(\text{proj}) / Q_s^2(\text{targ})$ weighted by the contribution to the gluon density.

Thus, it is interesting to simply run the IP-JAZMA calculation for $d+\text{Au}$ in the dense-dense case, and with no $Q_{s,0}^2$ fluctuations. The results are shown in Figure 13 and while capturing the overall shape of the data distribution, the agreement is certainly not as good as in the dilute-dense limit. Given that no parameters have been tuned, it is plausible that one could achieve a comparable level of agreement as found in the dilute-dense limit. This simply demonstrates that one can obtain roughly similar distributions either through fluctuations in the saturation scale of the projectile and a rather flat target or via a constant profile projectile and fluctuations in the nuclear thickness of the target. The latter case just validates the fact that the charged particle multiplicity approximately follows constituent quark scaling [44].

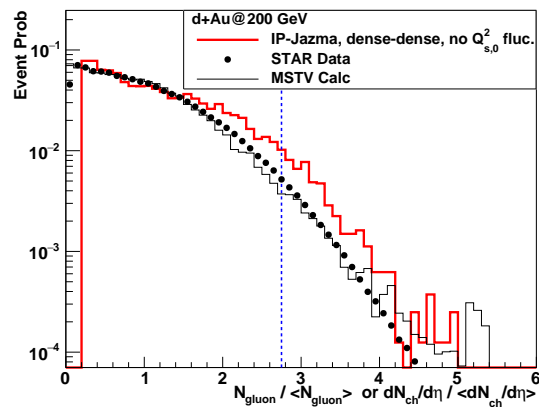


FIG. 13. IP-JAZMA $d+\text{Au}$ minimum bias results for the distribution of $N_g / \langle N_g \rangle$ in the dense-dense case and with no $Q_{s,0}^2$ fluctuations.

X. APPENDIX II

There is an interesting natural occurrence of negative binomial distribution (NBD) fluctuations within the Color Glass Condensate framework [39] – referred to as the “glittering glasma.” Subsequently, in a number of IP-Glasma and other papers, such NBD behavior is attributed to these gluon field contributions. However, there are many sources of fluctuations in the multi-step IP-Glasma and MSTV-type calculations. As a concrete example, Ref [12] uses the IP-Glasma framework to calculate the distribution of transverse energy (proportional to energy density) in a set of exactly impact parameter $b = 9$ fm Au+Au events at 200 GeV – see their Figure 1. The authors find that the distribution is not described by a Gaussian and rather has a positive skew better described by a NBD. (We note here that since energy is a continuous variable, this really should be a Gamma distribution.) We have studied the same test case using IP-JAZMA in the dense-dense limit to calculate the distribution of energy density in Au+Au events with fixed impact parameter $b = 9$ fm and plot the event-by-event distribution as shown in Figure 14. The red line is a Gaussian fit to the distribution, and reveals a clear positive skew in the IP-JAZMA result. Since there are neither fluctuations in $Q_{s,0}^2$ nor color or CGC-like fluctuations in this IP-JAZMA calculation, the gamma distribution skew relative to a simple Gaussian must have another source. That is to say, extreme caution should be used when at-

tributing positive skew in such distributions to intrinsic NBD properties of the CGC. It is clear from this example that mundane properties of sampling Monte Carlo Glauber configurations with Gaussian profiles produce similar features.

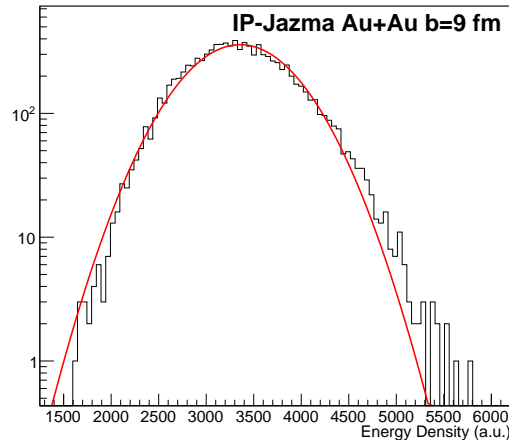


FIG. 14. IP-JAZMA Au+Au $b=9$ fm events at 200 GeV and their energy density distribution calculated in the dense-dense limit. Note that no $Q_{s,0}^2$ fluctuations are included. The red curve is a Gaussian fit to the distribution.

-
- [1] J. L. Nagle, A. Adare, S. Beckman, T. Koblesky, J. Orjuela Koop, D. McGlinchey, P. Romatschke, J. Carlson, J. E. Lynn, and M. McCumber, Phys. Rev. Lett. **113**, 112301 (2014), arXiv:1312.4565 [nucl-th].
- [2] C. Aidala *et al.* (PHENIX), (2018), arXiv:1805.02973 [nucl-ex].
- [3] K. Dusling and R. Venugopalan, Phys. Rev. Lett. **108**, 262001 (2012), arXiv:1201.2658 [hep-ph].
- [4] K. Dusling and R. Venugopalan, Phys. Rev. **D87**, 094034 (2013), arXiv:1302.7018 [hep-ph].
- [5] M. Mace, V. V. Skokov, P. Tribedy, and R. Venugopalan, (2018), arXiv:1805.09342 [hep-ph].
- [6] U. Heinz and R. Snellings, Ann. Rev. Nucl. Part. Sci. **63**, 123 (2013), arXiv:1301.2826 [nucl-th].
- [7] J. L. Nagle and W. A. Zajc, (2018), arXiv:1801.03477 [nucl-ex].
- [8] P. Romatschke and U. Romatschke, (2017), arXiv:1712.05815 [nucl-th].
- [9] K. Dusling, W. Li, and B. Schenke, Int. J. Mod. Phys. **E25**, 1630002 (2016), arXiv:1509.07939 [nucl-ex].
- [10] R. D. Weller and P. Romatschke, Phys. Lett. **B774**, 351 (2017), arXiv:1701.07145 [nucl-th].
- [11] V. Khachatryan *et al.* (CMS), JHEP **09**, 091 (2010), arXiv:1009.4122 [hep-ex].
- [12] B. Schenke, P. Tribedy, and R. Venugopalan, Phys. Rev. Lett. **108**, 252301 (2012), arXiv:1202.6646 [nucl-th].
- [13] H. Kowalski and D. Teaney, Phys. Rev. **D68**, 114005 (2003), arXiv:hep-ph/0304189 [hep-ph].
- [14] A. Dumitru and L. D. McLerran, Nucl. Phys. **A700**, 492 (2002), arXiv:hep-ph/0105268 [hep-ph].
- [15] M. L. Miller, K. Reygers, S. J. Sanders, and P. Steinberg, Ann. Rev. Nucl. Part. Sci. **57**, 205 (2007), arXiv:nucl-ex/0701025 [nucl-ex].
- [16] C. Loizides, J. Nagle, and P. Steinberg, SoftwareX **1-2**, 13 (2015), arXiv:1408.2549 [nucl-ex].
- [17] Note in this context x is momentum fraction, not a spatial coordinate. The additional factor of x in $xg(x, Q^2)$ converts $g(x, Q^2)$ to a gluon density per unit rapidity appropriate for these considerations of the saturation condition.
- [18] B. Schenke, P. Tribedy, and R. Venugopalan, Phys. Rev. **C86**, 034908 (2012), arXiv:1206.6805 [hep-ph].
- [19] A. Caldwell and H. Kowalski, in *Elastic and Diffractive Scattering. Proceedings, 13th International Conference, Blois Workshop, CERN, Geneva, Switzerland, June 29-July 3, 2009* (2009) pp. 190–192, arXiv:0909.1254 [hep-ph].
- [20] An alternative view is that this small radius characterizes the size of a constituent quark in the nucleon.
- [21] Also note that this value of B_G is for $x \approx 0.01$, appropriate for RHIC but not LHC energies.
- [22] K. J. Golec-Biernat and M. Wusthoff, Phys. Rev. **D60**, 114023 (1999), arXiv:hep-ph/9903358 [hep-ph].

- [23] E. Iancu, A. H. Mueller, and S. Munier, Phys. Lett. **B606**, 342 (2005), arXiv:hep-ph/0410018 [hep-ph].
- [24] C. Marquet, G. Soyez, and B.-W. Xiao, Phys. Lett. **B639**, 635 (2006), arXiv:hep-ph/0606233 [hep-ph].
- [25] L. McLerran and P. Tribedy, Nucl. Phys. **A945**, 216 (2016), arXiv:1508.03292 [hep-ph].
- [26] B. I. Abelev *et al.* (STAR), Phys. Rev. **C79**, 034909 (2009), arXiv:0808.2041 [nucl-ex].
- [27] T. Lappi, Phys. Lett. **B643**, 11 (2006), arXiv:hep-ph/0606207 [hep-ph].
- [28] C. Loizides, Phys. Rev. **C94**, 024914 (2016), arXiv:1603.07375 [nucl-ex].
- [29] J. S. Moreland, J. E. Bernhard, and S. A. Bass, Phys. Rev. **C92**, 011901 (2015), arXiv:1412.4708 [nucl-th].
- [30] S. McDonald, C. Shen, F. Fillion-Gourdeau, S. Jeon, and C. Gale, Phys. Rev. **C95**, 064913 (2017), arXiv:1609.02958 [hep-ph].
- [31] A. Bzdak, B. Schenke, P. Tribedy, and R. Venugopalan, Phys. Rev. **C87**, 064906 (2013), arXiv:1304.3403 [nucl-th].
- [32] B. Schenke and R. Venugopalan, *Proceedings, 24th International Conference on Ultra-Relativistic Nucleus-Nucleus Collisions (Quark Matter 2014): Darmstadt, Germany, May 19-24, 2014*, Nucl. Phys. **A931**, 1039 (2014), arXiv:1407.7557 [nucl-th].
- [33] B. Schenke, P. Tribedy, and R. Venugopalan, Phys. Rev. **C89**, 024901 (2014), arXiv:1311.3636 [hep-ph].
- [34] B. Schenke, S. Schlichting, P. Tribedy, and R. Venugopalan, in *27th International Conference on Ultrarelativistic Nucleus-Nucleus Collisions (Quark Matter 2018) Venice, Italy, May 14-19, 2018* (2018) arXiv:1807.05632 [nucl-th].
- [35] J. P. Blaizot, F. Gelis, and R. Venugopalan, Nucl. Phys. **A743**, 13 (2004), arXiv:hep-ph/0402256 [hep-ph].
- [36] J. P. Blaizot, F. Gelis, and R. Venugopalan, Nucl. Phys. **A743**, 57 (2004), arXiv:hep-ph/0402257 [hep-ph].
- [37] L. McLerran and V. Skokov, Nucl. Phys. **A959**, 83 (2017), arXiv:1611.09870 [hep-ph].
- [38] Cyrille Marquet, private communication.
- [39] F. Gelis, T. Lappi, and L. McLerran, Nucl. Phys. **A828**, 149 (2009), arXiv:0905.3234 [hep-ph].
- [40] C. Aidala *et al.* (PHENIX), Phys. Rev. **C96**, 064905 (2017), arXiv:1708.06983 [nucl-ex].
- [41] A. Adare *et al.*, (2018), arXiv:1807.11928 [nucl-ex].
- [42] B. Schenke, S. Schlichting, P. Tribedy, and R. Venugopalan, Phys. Rev. Lett. **117**, 162301 (2016), arXiv:1607.02496 [hep-ph].
- [43] K. Dusling, M. Mace, and R. Venugopalan, Phys. Rev. Lett. **120**, 042002 (2018), arXiv:1705.00745 [hep-ph].
- [44] A. Adare *et al.* (PHENIX), Phys. Rev. **C93**, 024901 (2016), arXiv:1509.06727 [nucl-ex].